THE ASTROPHYSICAL JOURNAL, 326:L31–L34, 1988 March 1

HERBIG-HARO OBJECTS AS SHOCKED AMBIENT CLOUDLETS—HIGH-RESOLUTION RADIO OBSERVATIONS OF HH 7–11

ALEXANDER RUDOLPH[1,2] AND WILLIAM J. WELCH[1]
Received 1987 September 28; accepted 1987 November 17

ABSTRACT

Observations of the region near the objects HH 7–11 were made with the Hat Creek millimeter interferometer. Aperture synthesis maps with 7″–8″ resolution of the HCO^+ ($J = 1 \rightarrow 0$) transition show a striking correlation of the peaks of line intensity with the positions of the optical HH objects. The velocities of the clumps of HCO^+ emission are comparable to the systemic velocity of the cloud ($|v - 8.2$ km s$^{-1}| \lesssim 1$ km s^{-1}) implying that the clumps are almost stationary. The narrow linewidths of the HCO^+ emission ($\Delta v \lesssim 0.5$ km s^{-1}) suggest that the clumps of emission are quiescent. This coincidence of quiescent *almost stationary* ambient gas with the fast-moving shock-excited HHs suggests that HH 7–11 are the shocked surfaces of stationary dense ambient cloudlets buffeted by a high-velocity stellar wind.

Subject headings: interferometry — nebulae: general — shock waves

I. INTRODUCTION

Herbig-Haro objects have been somewhat enigmatic in nature since their discovery in the early 1950's (Herbig 1951; Haro 1952). A major step forward in understanding HHs came with successful models suggesting that their optical spectra are caused by shocks (Dopita 1978; Raymond 1979). Since then many models for the origin of these strange objects have been put forth. Among these are the "interstellar bullet" (Norman and Silk 1979), the focused stellar wind (Cantó and Rodríguez 1980), and the shocked and possibly accelerated cloudlet (Schwartz 1978; Sandford and Whitaker 1983). None of these has been completely satisfactory (Schwartz 1983).

HH 7–11 are a string of HH objects associated with the young stellar object SVS 13 (Strom, Vrba, and Strom 1976) in the molecular cloud NGC 1333. Hα images by Mundt (1984) show that HH 7–11 are the brightest portions of an almost continuous structure extending from HH 11 to HH 7. The five HHs are observed to be surrounded by the blue lobe of a bipolar CO outflow (Snell and Edwards 1981; Edwards and Snell 1984), much the same as HH 28 and 29 in the classic CO outflow in L1551 (Snell, Loren, and Plambeck 1980). The HH objects lie approximately on a line and are also remarkably regularly spaced. The optical spectra of these HHs have been modeled as due to low-excitation shocks $v \lesssim 40$ km s^{-1} (Böhm, Brugel, and Olmsted 1983; Solf and Böhm 1987). Herbig and Jones (1983) have measured proper motions for HH 7–11 and find that only HH 11 has a measurable proper motion of 3″.5 per century directed away from SVS 13, 58 km s^{-1} at a distance to NGC 1333 of 350 pc.

Two groups (Zealey, Williams, and Sandell 1984; Lightfoot and Glencross 1986) have detected shock-excited H_2 from the region immediately surrounding HH 7–11 as well as to the northwest of SVS 13 in the direction of the red lobe of the CO flow. Two H_2O masers have been detected toward the region near HH 7–11 (Haschick *et al.* 1980), one coincident with SVS 13, the other ~30″ to the southwest. Grossman *et al.* (1987) observed this region and found that blueshifted ^{12}CO ($J = 1 \rightarrow 0$) is anticorrelated with the HH objects. Lizano *et al.* (1987) have observed HH 7–11 in the 21 cm transition of H I and find broad wings out to velocities of 170 km s^{-1}. They interpret these wings as a neutral component of a stellar wind driving the CO flow.

We have mapped the region near HH 7–11 in the $J = 1 \rightarrow 0$ transition of HCO^+ in order to study the distribution of dense gas in the vicinity of a young stellar object with associated HH objects. We here report the results of this project.

II. OBSERVATIONS

Observations were made with the Hat Creek millimeter interferometer between 1986 February and June. Data from five configurations of the three 6.1 m antennas were obtained, with baselines out to 90 m E–W and 80 m N–S. The total integration time was 74 hr. The point sources 0234P282, PK 0420, and 0528P134 were used as phase references. From the phase stability we estimate our absolute position accuracy to be at least ~1″. Observations of planets were used for flux calibration using planet brightness temperatures from Ulich (1981). Fluxes should be accurate to within 20%. System temperatures ranged from 300 to 800 K SSB scaled above the atmosphere, with a weighted average of 400 K for all the data.

A 512 channel digital correlator (Urry, Thornton, and Hudson 1985) was used to obtain cross correlation spectra of the 89.188523 GHz transition of HCO^+ with both 64 channels of 0.131 km s^{-1} and 64 channels of 0.526 km s^{-1} width. The high-resolution data were Hanning-smoothed so that the final resolutions are 0.262 km s^{-1} and 0.526 km s^{-1}.

The visibility data were convolved onto a grid, Fourier-transformed, and CLEANed in the usual way to produce maps. Natural weighting was used to generate a synthesized beam of 8″ × 7″.

III. RESULTS

Figure 1 (Plate L1) shows the HCO^+ emission superposed on an optical image of the region. The HCO^+ map was made by adding together all CLEANed channel maps which showed emission. A blanking cutoff of 2 $\sigma = 2.4$ K was used prior to adding the maps. The equivalent width of the map is 1.441 km s^{-1}. The six peaks of HCO^+ emission are labeled A–E and NW for the peak to the northwest of SVS 13. Peak C consists of two peaks at different velocities labeled C1 and C2. SVS 13 is represented by a square, and the two H_2O masers,

[1] Radio Astronomy Laboratory, University of California, Berkeley.
[2] Department of Physics, University of Chicago.

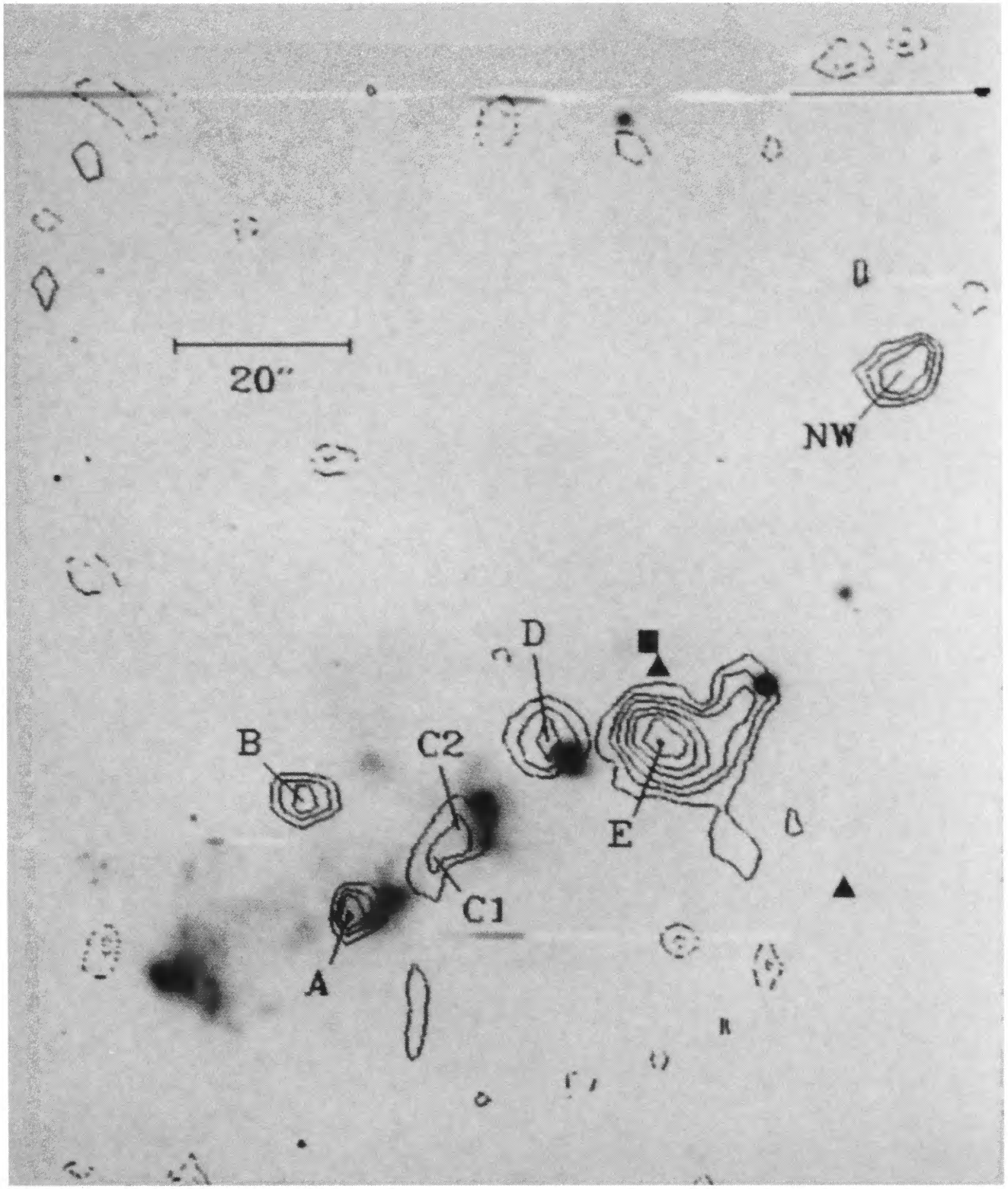

FIG. 1.—Integrated interferometer map (1.441 km s^{-1} width) of HCO^+ ($J = 1 \rightarrow 0$) emission overlaid on a CCD Hα image. The HCO^+ peaks are labeled A–E and NW. The contour levels are $(-3, -2, 2, 3, 4, 5, 6, 7, 8, 9) \times 0.37$ K (1 σ). Dashed contours are negative. The square represents SVS 13, and the two triangles represent H_2O masers.

RUDOLPH AND WELCH (*see* **326**, L31)

by triangles. Peaks A–D and NW are unresolved at a resolution of 8″ × 7″. Peak E, which has no optical counterpart, is ~11″ × 9″ which deconvolves to ~7″ × 6″.

It is striking to note that, with the exception of HH 7, there is an HCO^+ peak associated with each of the HH objects, two peaks in the case of HH 10. Also, the HCO^+ peaks are clearly downwind from HH 8–10. HCO^+ peak D is to one side of HH 11. This difference may be related to the proper motion of HH 11 and will be discussed in § IV*c*.

Figure 2 shows spectra for the seven peaks of HCO^+ along with a spectrum of blank sky for reference. Clearly the lines are extremely narrow, $\Delta v \lesssim 0.5$ km s^{-1}, indicating that the clumps are quiescent. Also, the emission comes from velocities within ~1 km s^{-1} of the systemic velocity of the cloud, indicating that these emission peaks are essentially at rest as well as internally quiet.

HCO^+ peak NW has a velocity of 9.1 km s^{-1} and is to the northwest of SVS 13 in the direction of the red lobe of the CO flow. The association of HCO^+ peaks with HH 8–11 suggests that HCO^+ peak NW is an invisible HH object undetected optically due to excessive obscuration towards the red lobe of the CO flow. This idea is confirmed by the presence of shock-excited H_2 (Zealey, Williams, and Sandell 1984; Lightfoot and Glencross 1986) to the northwest of SVS 13. Also the asymmetry of a lack of optical HH objects in the red lobe of CO is effectively removed.

The wider channels ($\Delta v = 0.526$ km s^{-1}) provide coverage from −8.8 to 22.2 km s^{-1}. There is no significant emission outside of $7.5 \lesssim v \lesssim 9.1$ km s^{-1}, above a peak noise level of 2.5 K, and at angular scales smaller than ~40″ (larger angular scales were not measured by the interferometer). This velocity range does not include the radial velocity ranges −70 to −50 km s^{-1} and −155 to −200 km s^{-1} of the optical HH objects (Solf and Böhm 1987). Observations of this wider range are in progress.

IV. DISCUSSION

a) The Properties of the HCO^+ Clumps

The HCO^+ peaks are remarkable in at least four ways.

1. The peaks have low velocities relative to the ambient cloud velocity ($|v - 8.2$ km s$^{-1}| \lesssim 1$ km s^{-1}). Thus the gas is stationary and therefore not part of the flow.

2. There is a correlation of the *almost stationary* HCO^+ with the fast-moving shock-excited HHs. This shows directly, for the first time, the interaction between material ejected from a young stellar object and the surrounding medium on such small scales (0.02 pc).

3. The HCO^+ peaks are *downwind* from the HHs. This morphology can be used to distinguish among competing theories of the formation of HH objects (see § IV*c*).

4. The narrow linewidths of the HCO^+ emission ($\Delta v \lesssim 0.5$ km s^{-1}) imply that they are internally quiet.

Beyond these basic facts a number of interpretations of these observations can be made. Section IV*b* gives estimates of the column densities of HCO^+, the density of H_2, and mass of these clumps. In § IV*c* we consider how the clumps of HCO^+ help reveal the nature of HH 7–11. In § IV*d* we consider the origin of the HCO^+ clumps.

b) Density, Mass, and Column Density

There are a number of ways to put limits on the density and mass of these clumps. Collisional excitation of HCO^+ requires an H_2 density greater than the critical density n_{crit} = few × 10^5 cm^{-3} (Vogel and Welch 1983). For $n = 2 \times 10^5$ cm^{-3} and clumps 7″ across, the mass is ~0.008 $M_\odot$.

Following Vogel and Welch (1983) the integrated intensity is used to calculate the number of HCO^+ molecules in each clump assuming the emission is optically thin. The mass of each clump is then calculated from $M = \mathcal{N}(HCO^+) m_{H_2} / X_{HCO^+}$, where $\mathcal{N}(HCO^+)$ is the number of

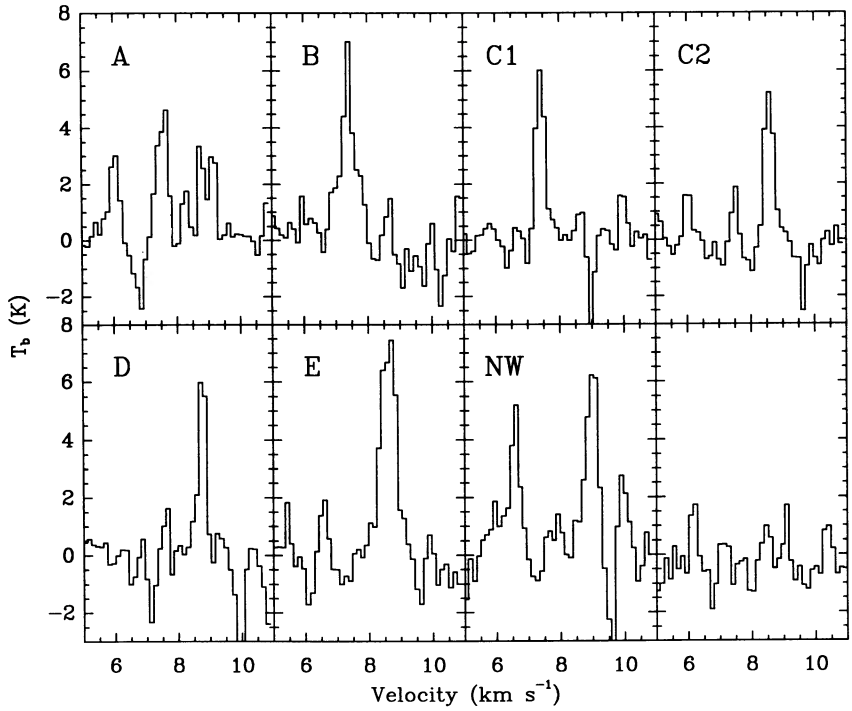

FIG. 2.—Spectra of HCO^+ peaks A–E and NW plus a spectrum of blank sky for reference

TABLE 1

PROPERTIES OF HCO^+ CLUMPS

Clump	α_{1950} ($\pm 0^s.1$)	δ_{1950} ($\pm 1''$)	$\int T_b\,dv$ (K km s^{-1})	$N(HCO^+)$ (cm^{-2})	Mass ($M_\odot$)
A	$3^h26^m00^s.9$	31°05′17″	0.92	0.6×10^{12}	0.6×10^{-3}
B	3 26 01.3	31 05 29	1.63	1.0×10^{12}	1.1×10^{-3}
C1	3 26 00.1	31 05 21	1.62	1.0×10^{12}	1.1×10^{-3}
C2	3 26 00.0	31 05 27	1.40	0.9×10^{12}	0.9×10^{-3}
D	3 25 59.3	31 05 37	1.65	1.0×10^{12}	1.1×10^{-3}
E	3 25 58.0	31 05 35	10.50	6.6×10^{12}	7.1×10^{-3}
NW	3 25 56.1	31 06 18	2.08	1.3×10^{12}	1.4×10^{-3}

HCO^+ molecules, and X_{HCO^+} is the abundance of HCO^+ relative to H_2.

Table 1 lists the integrated flux, the beam averaged column density [$N(HCO^+) = \mathcal{N}(HCO^+)/\Omega D^2$ where Ω is the beam size, and D is the distance], and the mass for each emission peak, assuming $X_{HCO^+} = 2.3 \times 10^{-9}$ (Blake *et al.* 1987). This method also gives masses of $\sim 10^{-3}\ M_\odot$ in rough agreement with the crude estimate based on the critical density. Both estimates are lower limits up to uncertainties in the abundance of HCO^+.

c) *The Nature of HH 7–11*

The simplest explanation of the HCO^+ peaks is that they are the dense stationary clumps which shock the high-velocity stellar wind, forming HH 7–11. This is consistent with the low velocities of the clumps as well as with the downwind position of the clumps relative to the HH objects. This latter point is important since the opposite is expected in a bullet model, where the *dense* projectile (the HCO^+ peak) would be *upwind* from the shocked ambient material (the HH object). Also, in the bullet model the dense object is moving at high velocity whereas the observed HCO^+ clumps are at rest.

One is left with the task of explaining the apparent proper motion of HH 11. Since HH 11 is to one side of HCO^+ peak D, which is slightly out of line with the apparent flow defined by the HH objects, the shock is presumably oblique. This idea is supported by the low derived shock velocity ($v = 40$ km s^{-1}) relative to radial velocity of HH 11 ($v = 146$ km s^{-1}) (Strom, Grasdalen, and Strom 1974). In the case of an oblique shock it may be reasonable to believe that the shocked material could move along the edge of the dense clump. An estimate of the mass of the optical object HH 11 follows from the electron density, ionization fraction, and size of the object ($n_e = 1300$ cm^{-3}, $f_e = 10\%$, $d \approx 2''$: Böhm, Brugel, and Olmsted 1983; Solf and Böhm 1987). These numbers give an HH mass of $6 \times 10^{-6}\ M_\odot$ which is negligible compared to the $10^{-3}\ M_\odot$ of the HCO^+ clump. Thus, the HH objects could easily be pieces of shocked wind which have broken off into the flow. It is unlikely that the wind could accelerate the HCO^+ clumps significantly since the clumps are denser than the wind by two to three orders of magnitude (Sandford and Whitaker (1983).

d) *The Nature of the Ambient Clumps*

The question remains: Why are the clumps seen in HCO^+ aligned with the wind with little evidence of emission elsewhere? There are at least two possibilities. The wind may enhance the abundance of HCO^+ in these clumps, raising the column density to an observable level. Alternatively these clumps may represent regions compressed by the wind to densities greater than n_{crit} for HCO^+.

A crude estimate of the HCO^+ abundance is obtained from

$$X\left(\frac{HCO^+}{H_2}\right) = \frac{N(HCO^+)}{N(H_2)} \approx \frac{N(HCO^+)}{D(\theta_M\,\theta_m)^{1/2} n_{crit}} \approx \frac{10^{12}}{10^{16}\,10^5} \approx 10^{-9},$$

where θ_M and θ_m are the major and minor beam axes (all other symbols are defined above). This is consistent with no enhancement, since Blake *et al.* (1987) find a fractional abundance of $(2\text{–}8) \times 10^{-9}$ in the quiescent regions of Orion, Sgr B2, and TMC-1.

Marginal observational evidence for enhancement within the HCO^+ clumps comes from the CS ($J = 2 \rightarrow 1$) maps also made with the Hat Creek interferometer (Rudolph and Welch 1988). There is no CS emission toward the HCO^+ peaks on these maps with an equivalent velocity and spatial resolution to the HCO^+ maps and rms noise level $\sigma = 1.19$ K. The HCO^+ peaks have brightness temperatures of $T_b \approx 6$ K indicating an overabundance of HCO^+ relative to CS of $\gtrsim 2$. Given the uncertainties in abundances, this is consistent with very modest or no enhancement; however, this is a lower limit.

The presence of a shock in the wind (the HH object) with a shock velocity of $v_s = 40$ km s^{-1} implies that there will be a secondary shock into the clump (Schwartz 1978). It is easy to show that in the presence of a magnetic field (Hollenbach and McKee 1979).

$$\frac{n_f}{n_0} = 76.7\,\frac{n_w^{1/2} v_{ws7}}{B_{0\perp -6}},$$

where n_f/n_0 is the compression of the clump, $n_w = 300$ cm^{-3} is the wind preshock density, $v_{ws7} = 0.4$ is the wind shock velocity in units of 100 km s^{-1}, and $B_{0\perp -6}$ is the magnetic field perpendicular to the shock direction in units of μG. Heyer, Strom, and Strom (1987) find from infrared polarimetry that the magnetic field direction near HH 7–11 is well aligned with the CO outflow. Some twisting of the field could occur on small scales; moreover, the shock is probably oblique. However, it is still likely that the field lines and the shock direction are lined up to $\sim 20°$. The field in dark clouds such as those found in Taurus and ρ Oph is on the order of 20 μG (Heiles 1987). In that case the compression is a factor of 75, enough to raise the ambient cloud density of $n = 10^4$ cm^{-3} (Lada *et al.* 1974) above the critical density for excitation of HCO^+. The crossing time for the shock is $\sim 10^3$ yr which is shorter than the lifetime of the flow. Therefore, this compression could account for the presence of the dense clumps along the wind axis.

V. SUMMARY

The conclusions of this paper are as follows:

1. There is HCO^+ emission on a 7″–8″ scale from the region near HH 7–11, mapped with the Hat Creek millimeter interferometer.

2. The HCO^+ peaks of emission are correlated with and *downwind* from HH 8–11.

3. The HCO^+ peaks have velocities close to the ambient cloud velocity ($|v - 8.2$ km s$^{-1}| \lesssim 1$ km s^{-1}). Thus, they are essentially at rest.

4. The HCO^+ peaks have narrow linewidths ($\Delta v \lesssim 0.5$ km s^{-1}), indicating that they are internally quiescent.

5. HCO^+ peak NW to the northwest of SVS 13 coincides with the red lobe of the CO flow and has a slight redshift ($v = 9.1$ km s^{-1}) with respect to the ambient cloud velocity ($v = 8.2$ km s^{-1}). This peak represents shock activity such as that seen in HH 7–11. This shock is seen in 2 μm H_2 emission (Zealey, Williams, and Sandell 1984; Lightfoot and Glencross 1986) but is unobserved optically due to the large extinction toward the red lobe of the CO flow.

6. The HCO^+ data support a picture in which HH 7–11 are the shocks formed on the upwind edges of dense, stationary, quiescent, ambient clumps. The presence of these clumps correlated with HH 7–11 can be explained as due to enhancement of their HCO^+ abundance (though the evidence for this is marginal), or to their compression by the wind to a density above the critical density for excitation of HCO^+, or to both.

Special thanks to Susana Lizano for many careful readings of the manuscript. We would also like to thank Dick Plambeck for suggesting HH 7–11 as an object for study, and Alex Raga and Mario Mateo for the use of their CCD image of HH 7–11. We also acknowledge many helpful discussions with Patricia Carral, Martin Cohen, Carl Heiles, Dave Hollenbach, Pat Palmer, and Frank Shu. Kate Ebneter provided invaluable technical assistance in preparing Figure 1. This work was supported by NSF grant AST-8616177.

REFERENCES

Blake, G. A., Sutton, E. C., Masson, C. R., and Phillips, T. G. 1987, *Ap. J.*, **315**, 621.
Böhm, K. H., Brugel, E. W., and Olmsted, E. 1983, *Astr. Ap.*, **125**, 23.
Cantó, J., and Rodríguez, L. F. 1980, *Ap. J.*, **239**, 982.
Dopita, M. A. 1978, *Ap. J. Suppl.*, **37**, 117.
Edwards, S., and Snell, R. L. 1984, *Ap. J.*, **281**, 237.
Grossman, E. N., Masson, C. R., Sargent, A. I., Scoville, N. Z., Scott, S., and Woody, D. P. 1987, *Ap. J.*, **320**, 356.
Haro, G. 1952, *Ap. J.*, **115**, 572.
Haschick, A. D., Moran, J. M., Rodríguez, L. F., Burke, B. F., Greenfield, P., and Garcia-Barreto, J. A. 1980, *Ap. J.*, **237**, 26.
Heiles, C. 1987, private communication.
Herbig, G. 1951, *Ap. J.*, **113**, 697.
Herbig, G. H., and Jones, B. F. 1983, *A.J.*, **88**, 1040.
Heyer, M. H., Strom, S. E., and Strom, K. M. 1987, *A.J.*, in press.
Hollenbach, D., and McKee, C. F. 1979, *Ap. J. Suppl.*, **41**, 555.
Lada, C. J., Gottlieb, C. A., Litvak, M. M., and Lilley, A. E. 1974, *Ap. J.*, **194**, 609.
Lightfoot, J. F., and Glencross, W. M. 1986, *M.N.R.A.S.*, **221**, 993.
Lizano, S., Heiles, C., Rodríguez, L. F., Koo, B., Shu, F. H., Hasegawa, T., Hayashi, S., and Mirabel, I. F. 1987, *Ap. J.*, submitted.
Mundt, R. 1984, in *Protostars and Planets II*, ed. D. C. Black and M. S. Matthews (Tucson: University of Arizona Press), p. 414.
Norman, C., and Silk, J. 1979, *Ap. J.*, **228**, 197.
Raymond, J. 1979, *Ap. J. Suppl.*, **39**, 1.
Rudolph, A., and Welch, W. J. 1988, in preparation.
Sandford, M. T., and Whitaker, R. W. 1983, *M.N.R.A.S.*, **205**, 105.
Schwartz, R. D. 1978, *Ap. J.*, **223**, 884.
———. 1983, *Ann. Rev. Astr. Ap.*, **21**, 209.
Snell, R. L., and Edwards, S. 1981, *Ap. J.*, **251**, 103.
Snell, R. L., Loren, R. B., and Plambeck, R. L. 1980, *Ap. J. (Letters)*, **239**, L17.
Solf, J., and Böhm, K. H. 1987, *A.J.*, **93**, 1172.
Strom, S. E., Grasdalen, G. L., and Strom, K. M. 1976, *Ap. J.*, **191**, 111.
Strom, S. E., Vrba, F. J., and Strom, K. M. 1976, *A.J.*, **81**, 314.
Ulich, B. L. 1981, *A.J.*, **86**, 1619.
Urry, W. L., Thornton, D. D., and Hudson, J. A. 1985, *Pub. A.S.P.*, **97**, 745.
Vogel, S. N., and Welch, W. J. 1983, *Ap. J.*, **269**, 568.
Zealey, W. J., Williams, P. M., and Sandell, G. 1984, *Astr. Ap.*, **140**, L31.

ALEXANDER RUDOLPH and WILLIAM J. WELCH: Radio Astronomy Laboratory, University of California, Berkeley, CA 94720